The origin of convective structures in the scrape-off layer of linear magnetic fusion devices investigated by fast imaging

G. Y. Antar, J. H. Yu, and G. Tynan
University of California San Diego, 9500 Gilman Drive, La Jolla, California 92093

A fast imaging camera is used to unveil the spatio-temporal properties of radially convective events in the CSDX linear plasma device [M. J. Burin *et al.*, Phys. Plasmas, **12**, 052320 (2005)]. The exposure time is set to 1 μs and the time between frames to 10 μs. The time series from a Langmuir probe and from a pixel in the 50000-frame movie are compared and cross-correlated. Excellent agreement between the two diagnostics is found for spatial scales greater than 2.5 mm. The fluctuations inside the main plasma column are found to change between different poloidal mode numbers as a function of time. Accordingly, the power spectra determined in these linear devices reflect the sum over these modes. Outside the main plasma column, avaloids are observed to remain attached to the main plasma, hence their behavior does not become independent of the dynamics inside the main plasma column. Avaloid properties, assessed from imaging, agree with Langmuir probes done on various devices, except that the radial length is found to be much larger than previously determined because the blob-shape assumption is not valid. The link between fluctuations inside and outside the main plasma column indicates that the nonlinear evolution of the $m=1$ poloidal mode number is responsible for the creation of avaloids. © *2007 American Institute of Physics*. [DOI: 10.1063/1.2424886]

I. INTRODUCTION

The understanding and characterization of turbulence in the scrape-off layer (SOL) of magnetically confined plasmas are important and may actually be crucial for ITER. This is because the SOL is the region where the plasma is in direct contact with the first wall, and high-intensity plasma fluxes were reported in the L-mode[1–8] and during edge-localized modes (ELMs)[9] in high confinement mode (H-mode) discharges. We have dedicated several investigations to unveil the different facets of the intermittency observed in the SOL of magnetic fusion devices. In Refs. 10 and 6, it was shown that intermittent events are not caused by self-organization of turbulence in the SOL but rather by nonlocal structures that have large scales and large radial velocities. In order to have a precise description of these structures, we called them *avaloids*,[6] denoting large spatial scale, that is, of the order of turbulence macroscale, large radial velocity, of the order of 1/10th of the sound speed, and encountered intermittently in the SOL. Often, these structures are also called blobs, as was the case in Ref. 11. Lately, however, the term "blob" is used to describe any type of structures inside or outside the last closed flux surface (LCFS), making the discussion rather vague and imprecise. Hereafter, blobs will denote rather circular-shaped cross-section structures that are in the SOL and disconnected from the main plasma. The universality of avaloids was shown with excellent agreement among four different devices, including the PISCES linear device in Ref. 7. Several studies, done, for example, on DIII-D,[12] TEXTOR,[13] and TJ-II tokamaks,[14] as well as on an LAPD linear plasma device,[15] confirmed the universality of the processes occurring in the SOL.

Avaloids are important for ITER-like devices since it is now agreed that their radial velocity is very large, reaching 1/10th of the sound speed. This allows the perpendicular transport to be competitive with respect to the toroidal one leading to a particle flux on the midplane of the same order of magnitude as on the target plates and even probably higher.[16] In ITER, the two regions are made of different materials, namely beryllium and carbon, and the effect of such structures in affecting the first wall is still under investigation.[17]

The first study of the origin of intermittency in linear devices was done on PISCES.[8] Two probes were used, one vertical and the other horizontal. It was shown that bursts in the far SOL, at 7 cm from the main plasma column with a radius of 2.5 cm, are correlated to a low-frequency mode inside the main plasma column. This was done using two statistical methods: cross-correlation and cross-conditional averaging. We concluded that avaloids are generated as a result of a nonlinear saturation of an edge instability.

This paper presents results of our continued effort to have a better understanding of the origin of intermittent structures in linear devices. On CSDX, the region between the chamber wall and the edge of the main plasma column will hereafter be called the SOL. The transition to turbulence by changing the axial magnetic field has been studied in detail.[18] The results presented here are in excellent agreement with those obtained on PISCES with respect to the origin of avaloids. Further details and more information are gained, however, using fast imaging as we are able to study the spatio-temporal behavior of the plasma inside and outside the main plasma column. The extrapolation to toroidal confinement devices is of course not straightforward, but since strong similarities exist between the various machines,[7,14] similar processes to the ones shown hereafter may be occurring.

It is worth briefly describing what is meant here by the SOL and the main plasma column and how the two regions compare to toroidal devices. The main plasma column describes the region where plasma is being produced by either wave heating, as is the case in CSDX, or electron heating, as is the case in PISCES. In linear devices, all the field lines are open, hence there is no equivalence between the main plasma column and the plasma edge (nor the SOL), even though similarities exist in the way turbulence behaves.[19] The SOL of linear devices, on the other hand, and tokamaks are actually similar in the sense that the field lines are open and the only source of particles and heat into this region is radial turbulent transport. The main remaining difference is the magnetic-field line geometry. In the case in which it does not play a major role, the SOL in linear and toroidal devices should be very close, as was shown in Ref. 7.

This paper continues as follows. The experimental setup is discussed next, where the linear plasma device is described as well as the fast imaging camera. Section III illustrates the comparison between Langmuir probes and light intensity fluctuations showing that the two diagnostics present excellent agreement for low-frequency, hence large-scale fluctuations, while poor agreement is obtained for high-frequency small-scale fluctuations. In Sec. IV, we characterize the fluctuations inside the main plasma column showing that various modes with different numbers are excited and the fluctuations transit from one poloidal mode to another after a relatively long period of time. Section V is dedicated to the characterization of avaloids in the SOL of CSDX. Before concluding, Sec. VI shows that avaloids are associated primarily with the $m=1$ poloidal mode number confirming that they result from a nonlinear saturation of an edge instability.

II. THE EXPERIMENTAL SETUP

CSDX is a linear device with plasma generated by an $m=0$ helicon wave source at 13.56 MHz at a power of 1500 W.[18] During operation, the reflected power remained less than 10 W. Equally spaced coils produce a magnetic field with intensity that can be changed between 200 and 1000 G. Most of the measurements and results are obtained at $B\simeq900$ G. The full length of the chamber 2.8 m is used in this experiment where the end-plate is the glass Pyrex window at the end of the machine to allow axial imaging. The diameter of the CSDX chamber is about 20 cm, whereas the bell-jar, where the source is, is roughly 10 cm. The gas neutral pressure of argon is 3 mTorr (about 0.4 Pa) flowing at a rate of 15 sccm. A schematic of CSDX is given in Fig. 1(a).

The main diagnostic of this paper is the Phantom V7 camera used with the exposure time set to 1 μs and the between frames to 10 μs. The number of pixels is 64×64. Depending on the different lenses that can be freely used since the camera is outside the vacuum chamber, the selected pixels can cover an area of 5×5 cm^2 with a 50 mm lens to an area of 10×10 cm^2 using a 25 mm lens; the f number is 1.2 for the two lenses. The spatial scales reported hereafter are determined at the distance 1.7 m from the camera where the Langmuir probe is and upon which the camera is focused. No interference filter is being used, so the whole
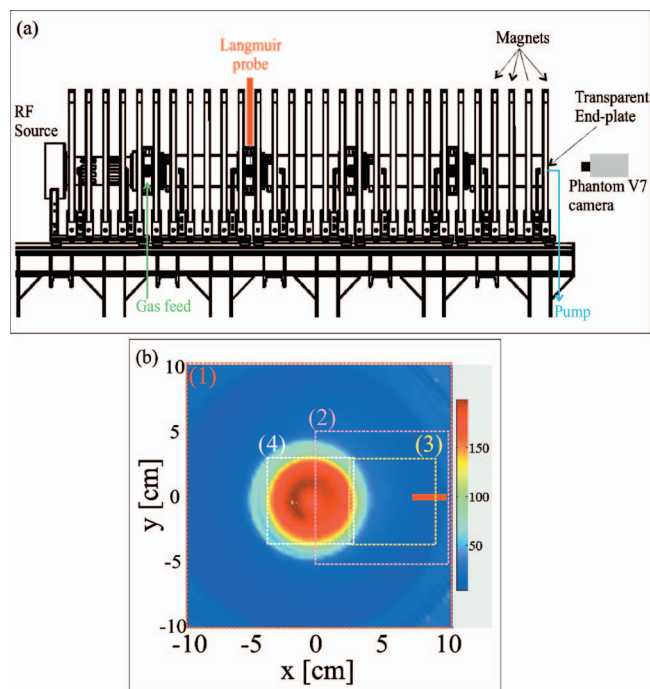

FIG. 1. (Color) (a) illustrates a schematic of linear plasma device along with the camera and the Langmuir probe. In (b) is shown a time-averaged image (over 2000 frames) of the plasma and the SOL. The main plasma occupies the center of the image. The blueish region around the red region is caused not only by the plasma but also by reflections in the bell-jar around which the rf antenna is installed. The position of the Langmuir probe is indicated and the various views that will be used hereafter are numbered from 1 to 4.

wavelength spectrum is included. More details about the turbulent structures can thus be obtained and the inside and outside regions of the plasma will be studied independently before connecting them together. The four different views used hereafter are shown in Fig. 1(b) and numbered from 1 to 4. Also shown is the position of the Langmuir probe.

III. COMPARING THE LIGHT-INTENSITY FLUCTUATIONS FROM THE FAST IMAGING CAMERA TO THE ION SATURATION CURRENT FLUCTUATIONS FROM A LANGMUIR PROBE

The various properties of avaloids studied on PISCES or other fusion devices were done using mainly Langmuir probes. Therefore, before showing the main results of this paper using imaging, we aim first at comparing the fluctuations measured by a Langmuir probe biased toward the ion saturation current (I_s) to those using the high-speed camera (I_c). The ion saturation current is proportional to the density and the sound speed $I_s\sim nT^{1/2}$, whereas the light intensity is proportional to nT^α, where α is about 3/4. Accordingly, neglecting the temperature fluctuations, both diagnostics reflect mainly the density fluctuations. Hereafter, though, we shall not make this assumption and we shall deal with the ion saturation current and light-intensity fluctuations. A Langmuir probe is inserted into the SOL of CSDX up to a distance of about 6 cm from the center (2.5 cm from the plasma edge). Its trigger is synchronized with that of the fast camera. The acquisition frequency is set to 1 MHz, however, for comparison purposes, only 1 out of 10 points is used as the
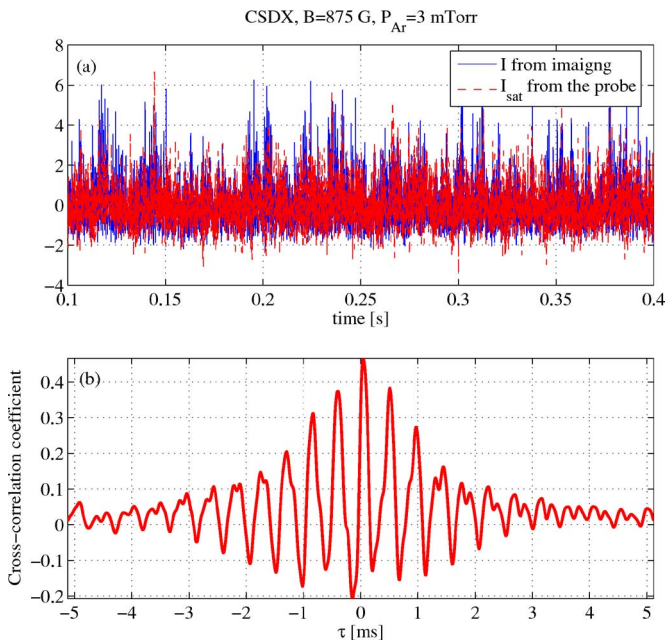
FIG. 2. (a) illustrates the raw ion saturation signal from the Langmuir probe and the signal from the light-intensity fluctuations of a pixel as a function of time. In (b), we plot the cross-correlation coefficient between the probe and the camera signals.

camera is operating at a rate of 100000 frames/s. One time series is thus the ion saturation current from the Langmuir probe. The light intensity at a pixel viewing an area that is a few millimeters from the probe is used to obtain the other time series. The number of images used in the comparison between the probe and the camera is 50000. The camera view #3 is used for this comparison where we image the SOL of CSDX.

A. Cross-correlating imaging and probe fluctuations

Figure 2(a) shows the raw signals from the two diagnostics, the camera I_c and the Langmuir probe I_s. One can note by visual inspection that rather good correlation exists between them. High-intensity bursts appear on both diagnostics but the details are often different. The cross-correlation coefficient offers a reliable and quantitative measurement of the correlation between the two signals. The average values of I_c and I_s are subtracted from the time series before performing the cross-correlation coefficient defined as

$$C(\tau) = \frac{\langle I_s(t)I_c(t+\tau)\rangle}{\sqrt{\langle I_s^2\rangle\langle I_c^2\rangle}}.$$

In Fig. 2(b), $C(\tau)$ is plotted where the amplitude reaches 0.5 at $\tau \simeq 0$. The decay time of this cross-correlation is about 2 ms reflecting a high correlation level for long times. The correlation amplitude being high but not close to unity is interpreted as a consequence of the contribution of small scales that are not correlated. We will actually confirm this in the next section.
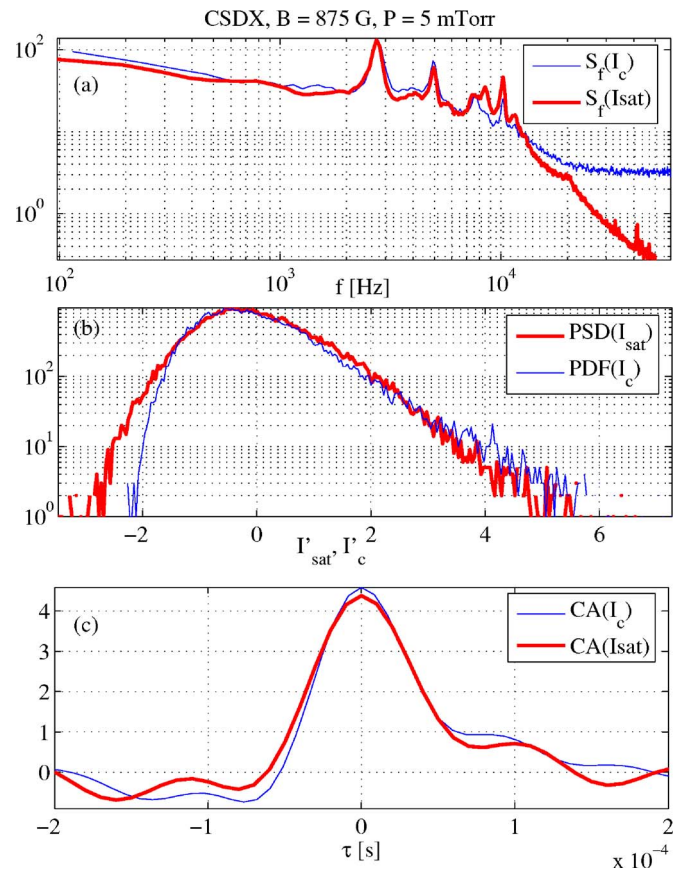

FIG. 3. (a) shows the frequency spectra of the time series deduced from the probe (I_s) by a thick solid line and movies (I_c) by a solid line. The two signals were normalized to their respective standard deviation. The probe is biased to the ion saturation current and one pixel is used from the images at a position close to the probe. The two signals are normalized by their standard deviation after subtraction of the average. The two graphs are in good agreement for frequencies smaller than 20 kHz. This is not the case for higher frequencies. In (b) is plotted the probability distribution functions of the two signals. There is good agreement for large positive intensities and poor agreement with negative ones. In (c) is plotted the autoconditional average for both signals. Excellent agreement is recorded as it reflects mainly large-scale events.

B. Comparing the statistical properties of the fluctuations by probes and imaging

In this section, we use three different statistical analyses to compare the two signals. The first is the power spectrum defined as the Fourier transform of the autocorrelation function, the second is the probability distribution function (PDF), and the third is the autoconditional average.

The comparison of the power spectra of the probe and camera signals, $S_f(I_c)$ and $S_f(I_s)$, is shown in Fig. 3(a), where the signals were normalized to their standard deviation. As the fluctuations have an average poloidal velocity, one can interpret the low-frequency part as caused by large-scale structures whereas the high-frequency component by small scales. The spectra are formed of spikes reflecting coherent fluctuations on top of a broadband component that reflects the incoherence of turbulent fluctuations. For low frequencies, mainly $f < 20$ kHz, the two diagnostic are in good agreement. In the high-frequency part, $f > 20$ kHz, this agreement is poor. This indicates that relatively large-scale

structures are equally resolved by the two diagnostics; this is not the case for small scales, where the level of fluctuations is below the instrumental noise.

The spatial resolution of the probe is set by its size. Fluctuations that are smaller than the size of the probe, about 1 mm^2, are averaged out and no information can be gained on their properties. Scales only larger than the probe size are resolved. For the camera, it is a more complicated story. The first source of limited spatial resolution is set by the pixel size and the area it is viewing. This has the same effect as the probe dimension. In our setup, this resolution is about 1 mm^2 for each pixel. The second source of limited resolution is the smearing that occurs as structures traveling at high speed are imaged. With 1 μs integration time, an object traveling at a speed of 5×10^4 cm/s yields a resolution of 0.5 mm. The third source of limited spatial resolution is the line integration. The camera being installed at the end of CSDX performs a line integration that has a small angle with respect to $k_\parallel$. This resolution is hard to accurately determine since it depends on various parameters such as the distribution of the light intensity in the plasma device and the focusing properties of the different lenses. However, from the power spectrum, one can deduce an effective spatial resolution of the camera that includes all of the three sources discussed above. As will be shown hereafter, the average poloidal velocity is about 5×10^4 cm/s. The cutoff frequency being 20 kHz leads to a spatial resolution of the images for each pixel about 2.5 mm. Consequently, scales above 2.5 mm are well resolved by the two diagnostics; this is not the case for scales smaller than 2.5 mm.

Figure 3(b) shows in a semilogarithmic plot the PDF of the ion saturation current fluctuations (I_s) as well that of the light-intensity fluctuations (I_c). The average value of the two signals was put to zero by subtracting the mean; then we normalized by the standard deviation. The two PDF's have the same feature as those published earlier on PISCES[7] or on other devices.[13,15] Note that fluctuations with intensity greater than zero agree rather well when measured by the two diagnostics. As was shown on several devices, this part of the PDF is dominated by the large-scale convective structures in the SOL called avaloids (or blobs). This is in agreement with the power spectra results, showing that the large scales are equally resolved by the two diagnostics. For negative fluctuations, however, this is not the case. The PDF of the ion saturation current shows events with negative amplitude that are higher than the images. Reflected in the parabolic shape of this side of the PDF, it was argued that negative fluctuations are mainly Gaussian perturbations.[10] The disagreement between the two diagnostics is interpreted as the contributions of the small scales (but with large amplitudes) that are not resolved by the imaging camera. This automatically leads to a narrower PDF for negative fluctuations caused by the "filtering" process as is observed.

In Fig. 3(c) is shown two autoconditional averaging curves of the time series. We recall that in order to obtain these curves, maxima above 2.5 times the standard deviation are selected. Then, an average is performed over the number of maxima.[8] We also recall that the two time series from the probe and the fast imaging were selected from the SOL. The

two diagnostics yield similar curves, which shows, as on PISCES and on tokamaks, a rather rapid increase of the intensity, in about 5×10^{-5} s, and a slow decrease in about 15×10^{-5} s. This is also consistent with the above results from the power spectra result, indicating that large time scales, and thus spatial scales, are well resolved by the two diagnostics.

We deduce that the light-intensity fluctuations and those measured by the probes have good correlation and that spatial scales above 2.5 mm are well resolved by the two diagnostics. This section allows us to link between the results that are presented hereafter using mainly fast imaging and those performed earlier using mainly Langmuir probes.

IV. DYNAMICS INSIDE THE MAIN PLASMA COLUMN

The main goal of this paper is to describe the origin of avaloids on CSDX. It is of importance to describe properties of the fluctuations inside the main plasma column that are in relationship with the generation of avaloids. The camera is now focused on the main plasma with view #4 in Fig. 1(b) using a 50 mm lens. The magnetic field is 875 G and it was verified that as long as $B > 500$ G, the results are qualitatively unchanged.

In Fig. 4, eight images of the main plasma column are shown that are 30 μs apart. In order to obtain this figure, we first performed a time average image from 2000 frames. It was verified that this number of images is sufficient to achieve statistical convergence. Then, each frame is subtracted from the "time-averaged image." In this case, even $m = 0$ spatial fluctuations can be resolved since we do not perform spatial integration. This sample set of images shows how the fluctuations inside the main plasma column transit from one poloidal mode number to another. At $t = 0$, an $m = 1$ mode is seen with two lobes corresponding to positive and negative density fluctuations. This mode is then destabilized gradually to reach an $m = 3$ poloidal mode number at $t \simeq 150$ μs. It thus takes a relatively long time to transit from one mode number to another. This type of behavior occurs all the time as one watches the movies taken on CSDX.

One rather important corollary that can be drawn from these images is that the average power spectrum often determined in these devices reflects the different modes that are occurring at different times in the plasma. It may have been thought that fluctuations possess a complex frequency spectrum that is there all the time and is reflected in the average power spectrum. The present results indicate that not all of the modes are present all of the time, but rather one mode is present at a given time and this mode is changing. The role of the nonlinearities in this case is not only to excite some modes but also to make the plasma transit from one mode number to another. The origin of this rather slow evolution of the spectrum is not understood at present and will be the subject of future investigations.

On several accounts, the average poloidal velocity of the plasma was mentioned in this paper. To accurately determine the dependence of the poloidal velocity on the distance to the plasma center, r, we select eight points that are at the same
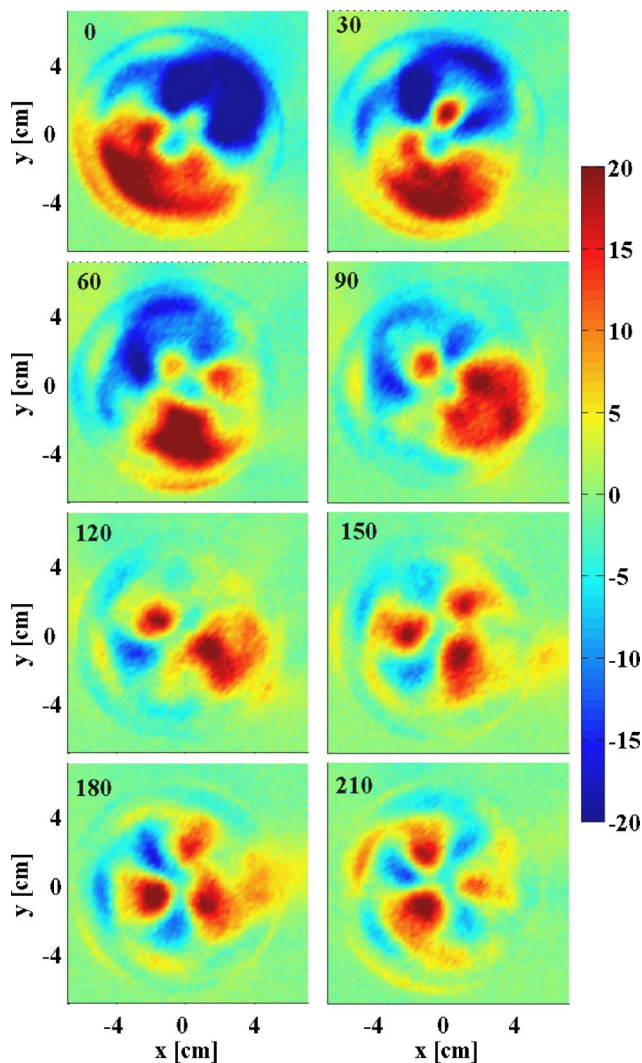
FIG. 4. (Color online) Eight images that are 30 μs apart from the same movie showing the fluctuations inside the main plasma column changing from an $m=1$ to an $m=3$ poloidal mode number. The view #4 is used where we zoom on the main plasma column.
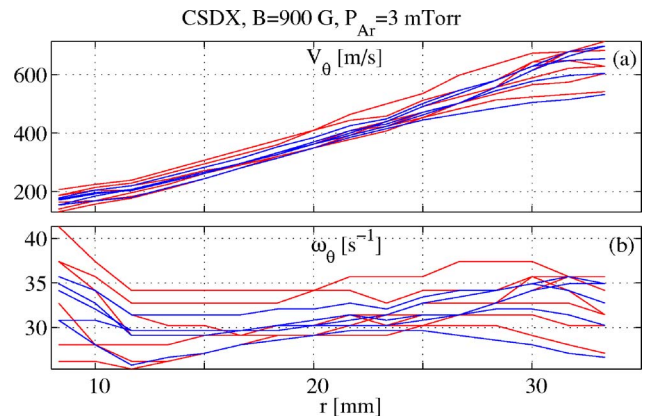

FIG. 5. In (a) we show the poloidal average velocity determined by cross-correlating the fluctuating light-intensity signals from different poloidal angles and for different radial positions. Note the linear increase with respect to the radial position inside the main plasma column that reflects a solid body rotation. In (b), we illustrate the rotation frequency, which is the same for all radii shown here.

main plasma column and in the case where the density fluctuations are affected by their dynamics.

V. DYNAMICS OF AVALOIDS IN THE CSDX SCRAPE-OFF LAYER

The main goal of this section is to provide information about avaloids using high-speed imaging to complement the probe results. It turns out, as will be shown hereafter, that a new "image" of avaloids is formed with shapes that are more finger-like that remains connected to the main plasma column rather than blob-like structures where they are disconnected.

A. Images of avaloids

Using the 25 mm lens and looking at the whole main plasma column with the SOL with view #1 in Fig. 1(b), Fig. 6 shows nine images. The integration time is set to 1 μs and the time between frames is 20 μs. In order to obtain these images, an average image is calculated from about 2000 frames; then each image is subtracted from the average one.

To our surprise, the convective structure observed in the SOL of CSDX remains attached to the plasma and does not form a blob but is rather *finger-like*. The structure is moving in the radial and poloidal directions bulging out of the main plasma column at a radial speed of about 10^5 cm/s. This is in excellent agreement with the probe measurements done on PISCES and also on toroidal devices. Furthermore, the structure is moving in the poloidal direction at a rate of about 5 $\times 10^4$ cm/s. This velocity is about the same in the main plasma column, but when divided by the distance to the center, it leads to a smaller poloidal rotation. The fact that the poloidal velocity of avaloids slows down as they are ejected into the SOL was verified statistically but not shown here. The finger-like shape remains until the structure disappears from the SOL.
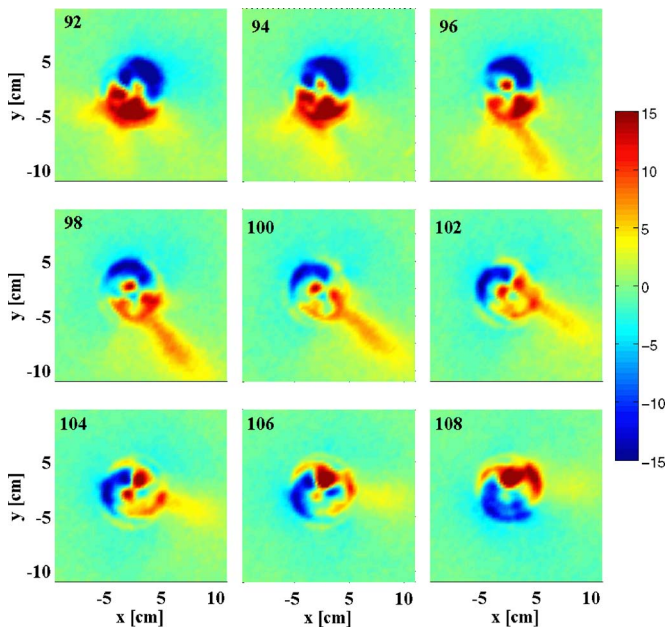
radius from the plasma center and perform cross-correlation. The poloidal velocity leads to a time shift. Knowing the poloidal distance between the selected points and the time shift, we deduce the poloidal speed. The cross-correlation between points that are an angle of $\pi/8$ and $\pi/4$ apart are then determined and shown in Fig. 5. A linear increase of the poloidal velocity with the radius is observed, reflecting a solid body rotation at a rate of 3200 s^{-1}. Even by increasing the radial resolution, no shear is observed in the plasma core using this time-delay method. For radii about 4 cm, the reflections in the bell-jar that can be seen in Fig. 4 disable us from making accurate determination of the poloidal velocity. However, when large plasma structures are radially transported out, the light coming from the plasma will dominate and the poloidal velocity determination is possible.

From the movie, no sign of a band or bands of density fluctuations that have an $m=0$ poloidal mode number was observed inside the main plasma column. These bands would have resulted from the presence of zonal flows inside the

FIG. 6. (Color online) Nine images with a time between frames set to 20 μs showing a sample of an avaloid birth, propagation into the SOL and decay. All the images have the same color-bar. View #1 is used.

B. Statistical properties of avaloids from the movies

The view of the camera is set to #2 in Fig. 1(b), where it is looking at not only the SOL, but also including almost half of the main plasma. The aim is to complement the information above by providing the statistical properties of avaloids from the 50000 frames. While analyzing the time series, we chose the conditional averaging method in order to study a specific type of fluctuations more or less independently from the background turbulence.[8,16,20] Here, we do the same but with movies. We first record a time series of 50000 points from the fluctuations at a pixel in the SOL from the whole movie. Maxima above 2.5 times the standard deviation are then selected from this time series. They are separated by a minimum of 5 frames. For each retained maximum, a short movie is then recorded with 10 frames before and 10 frames after it occurs. If N_{max} is the number of maxima selected in the time series, this is also the number of movies obtained. Finally, we average frame-by-frame all the movies together in order to obtain a conditionally averaged movie (CAM) that describes, on the average, the fluctuations that lead to high-intensity bursts. In this section, the position of the pixel selected to determine the maxima lies on the right-hand side of the plasma SOL near the probe.

A contour plot of the CAM is shown in Figs. 7(a) and 7(b); the total number of maxima above 2.5 times the standard deviation is 186. Only one contour is determined at half the maximum intensity in each image, and different colors correspond to different times in this CAM. The origin of time corresponds to the time just before the onset of the avaloid, so $t=0$ means no avaloid is present yet. In Fig. 7(a), one can note the fast radial ejection of the plasma occurring at a speed about 10^5 cm/s. Note that this velocity is not constant but varies during the expulsion. The radial velocity temporal evolution shows an early acceleration of the structure radi-
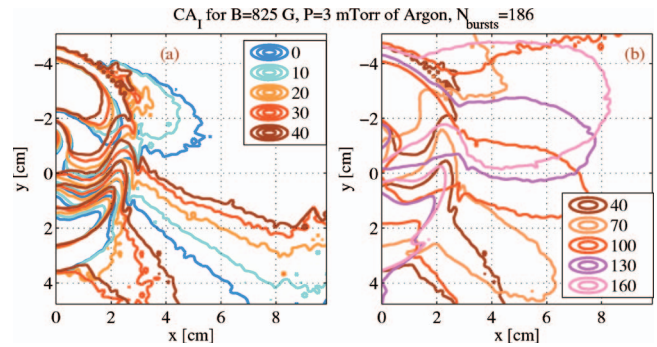

FIG. 7. (Color) Contours at half the maximum of light intensity in the image at different times of the conditional average movie (CA$_l$). The various times and corresponding colors are indicated in the legends. In (a) the plot shows the onset of an "average" avaloid and in (b) one can deduce its poloidal propagation, lifetime, and spatial extension. View #2 is used here.

ally outward and then a decrease toward zero, in good agreement with the probe measurements published earlier.[7] Despite this acceleration and the large radial velocity, the avaloid in CSDX remains attached to the main plasma column and there is no formation of a blobby structure. Consequently, there remains a link between inside and outside the main plasma column. This is a major modification of our "image" of avaloids (or blobs) as they were viewed as coherent plasma structures that are ejected from the main plasma and thus at some point become independent of the dynamics inside the main plasma column. The burst intensity decrease, reported by the probes, is thus caused not only by the velocity of propagation past the probes but also by the fact that the underlying instability is no longer *feeding* the SOL with plasma. Hence, on top of radial and poloidal propagation, there is a dynamic of growth and decay of avaloids in the SOL that should be taken into account while analyzing the probe data. The lifetime of avaloids does not depend on the properties of the SOL alone but includes the properties of the instability occurring inside the main plasma column.

From Fig. 7(b), one can determine the main properties of avaloids inserted in Table I. They are in excellent agreement with previous results except for the radial length scale. The latter was previously underestimated because the assumption of a blob passing by the probe is not valid.

Table I describes the different properties of avaloids deduced from the CAM.

TABLE I. The avaloid radial velocity ($V_{r,\text{avaloid}}$), poloidal velocity ($V_{\theta,\text{avaloid}}$), radial scale length ($L_{r,\text{avaloid}}$), poloidal scale length ($L_{\theta,\text{avaloid}}$), lifetime, and average time between bursts (ΔT) are shown.

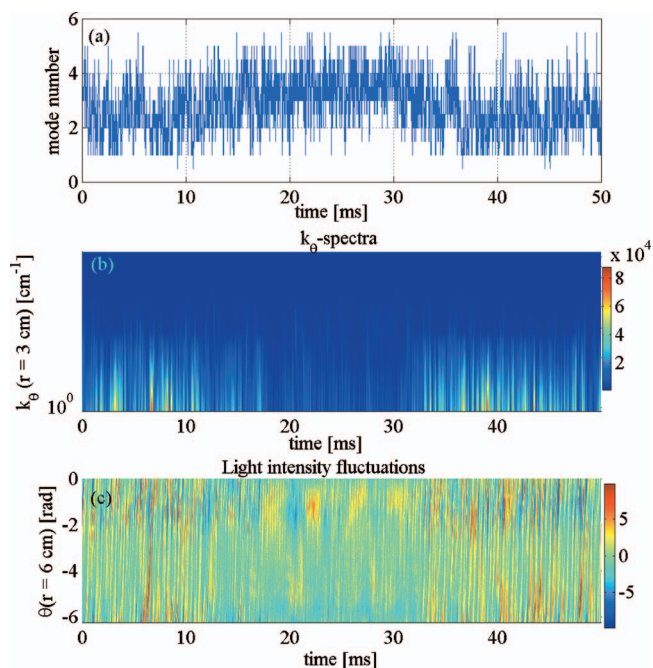|	
$V_{r,\text{avaloid}}$	2.3×10^5 cm/s
$V_{\theta,\text{avaloid}}$	5.3×10^5 cm/s
$L_{r,\text{avaloid}}$	5 cm
$L_{\theta,\text{avaloid}}$	2 cm
Lifetime	50 μs
ΔT	200 μs

FIG. 8. (Color) (a) illustrates the poloidal mode number determined by a ninth-order polynomial fit as a function of time. (b) shows the k_θ spectra that one can deduce from Fourier transform of the poloidal cuts in each image. In (c) is shown the fluctuations in the SOL of CSDX in arbitrary units as a function of time and the poloidal angle.

VI. ORIGIN OF CONVECTIVE TRANSPORT AND THE RELATION BETWEEN FLUCTUATIONS OUTSIDE AND INSIDE THE MAIN PLASMA COLUMN

The previous two sections were devoted to the properties of the plasma inside and outside the main plasma column. We have learned that inside the main plasma, a given poloidal mode exists for some time before it is replaced by another one. In the SOL, we have determined avaloid properties and have shown that they do not detach from the main plasma but stay attached with a finger-like shape. In this section, we aim at linking the two areas together in order to understand the origin of avaloids. We shall give three studies that show that avaloids are associated with low poloidal numbers and in particular to the $m=1$ one. In this study, it is mostly view #1 that is used, where the whole main plasma column as well as the SOL are imaged.

A. The link between low poloidal mode numbers inside the main plasma and the high level of fluctuations outside the main plasma

Two ways are used to show the link between the far SOL and the dynamics of the plasma inside the main plasma column. The first method consists of making a poloidal cut in the light intensity fluctuations in each image after subtracting the time-averaged one. This cut is performed *inside* the main plasma column. Next, a ninth-order polynomial fit is determined. This filters out the small-scale fluctuations and enables us to have the number of maxima and minima in each poloidal cut. An assessment of the poloidal mode number is thus readily obtained. The result is illustrated in Fig. 8(a), where the x axis is time and the y axis is the poloidal mode

number for the 50000 images. One can note that the poloidal mode number fluctuates between 1 and 5 in agreement with the sample of images presented in Fig. 4. The fluctuations of the poloidal mode number have a high-frequency component of the order of 20 kHz and a low-frequency one about 50 Hz. The source of the low-frequency component is not yet known.

The second more conventional method determines the k_θ spectrum by performing a Fourier transform of the fluctuations of a poloidal cut inside the plasma. The result is shown in Fig. 8(b), where the x axis is time, the y axis is k_θ, and the z axis is the amplitude of the power spectrum. The result is in good agreement with the polynomial fit method also showing the two components of the poloidal mode number temporal fluctuations. In the k_θ spectrum, the low m leads to a rather coherent spectrum with a peak at some given frequency, whereas high m leads to less spiky but more spread out spectrum. This is reflected in the color variations of Fig. 8(b).

In Fig. 8(c), we illustrate the poloidal cut but outside the main plasma column in the far SOL. The x axis is time, the y axis is the poloidal angle, and the z axis reflects the amplitude of the light-intensity fluctuations. Strong light-intensity fluctuations are observed to occur when the fluctuations inside the main plasma column have a low poloidal m number. This is clearly seen if one compares the times around 7 and 25 ms. Around 7 ms, the poloidal mode number inside the plasma determined by the above two methods is low, at the same time high-intensity fluctuations are recorded in the SOL. Around 25 ms, the poloidal mode number is high and the fluctuations in the SOL are nearly absent.

From Fig. 8, one can safely deduce that there is a link between the low poloidal m numbers and the ejection of avaloids in the SOL.

B. Avaloid generation and the $m=1$ poloidal mode number

We recall that it is the view #1 that is being used. In order to investigate the poloidal mode number linked to the generation of avaloids, we use the conditional averaging method described above (CAM). Figure 9 shows 16 consecutive images from the conditionally averaged movie. In the middle is the main plasma column surrounded by the SOL. From frames 1 to 8, one can see the onset of an $m=1$ mode rotating poloidally in the counterclockwise direction. The intensity of the mode is growing in time. From image 9, the onset of a convective structure is observed, reflecting the fact that there is a threshold of the $m=1$ mode amplitude. From subimages 10 to 16, we see the ejection of plasma outside the main plasma column at a large radial velocity. The plasma and the ejected structure remain linked and rotating poloidally. Figure 9 provides rather straightforward proof that avaloids in the SOL of CSDX are generated when the poloidal number $m=1$ is established inside the main plasma and when the consequent fluctuations exceed a certain threshold of intensity. This is in striking agreement with the PISCES results showing correlation between the far SOL and a mode inside the main plasma.[8] We want to emphasize that the above results of Fig. 9 were checked for different but
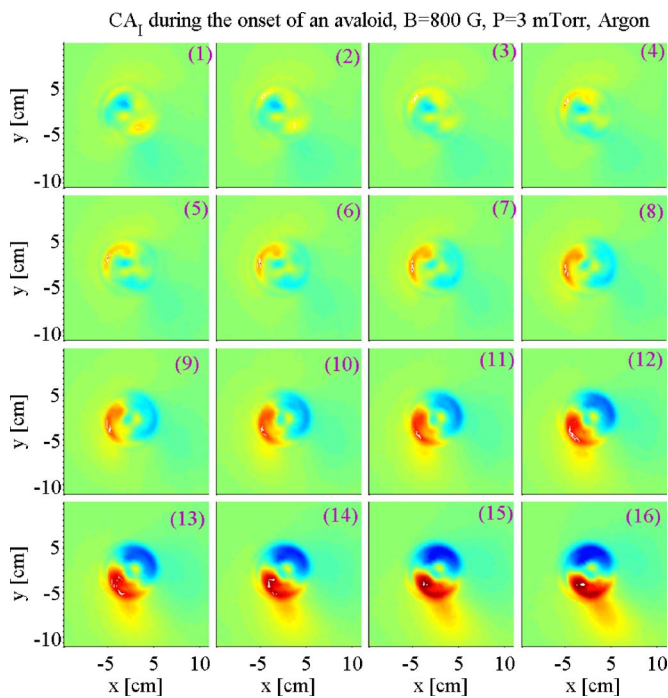
FIG. 9. (Color online) All the images are first subtracted from a temporal-average one using view #1. After performing the conditional average over all the high-intensity spikes in the SOL near the Langmuir probe, the average conditional movie is shown as a function of time. Note that first there is the onset of an $m=1$ mode number, it rotates, and then when it reaches a certain intensity the onset of an avaloid is observed.

FIG. 10. The x axis of all the figures denotes the poloidal mode number deduced from the ninth-order polynomial fit for the fluctuations inside the main plasma column. The y axis is the fluctuations in the SOL at a given poloidal position normalized by the standard deviation of the signal. The subplots (a)–(l) show the evolution of the two quantities as a function of the axial magnetic field. The onset of avaloids occurs for $B \sim 600$ G.

large magnetic fields ($B>600$ G). Also, we checked the results against the position of the pixel where the initial selection of high-intensity bursts is made.

C. Cross-correlating fluctuations outside to inside the main plasma column at different magnetic fields

The above results were obtained at a magnetic field equal to 850 G. We aim now at showing the same results but in a different way that also enables us to see the effect of the main magnetic field strength. We recall that in Ref. 18, the magnetic field was used to study the onset of turbulence on CSDX. When B was increased, the poloidal velocity decreased stabilizing the Kelvin-Helmholtz instability. At the same time, the stabilizing effect of the ion Larmor radius decreases while higher plasma pressure is achieved, allowing the onset of a drift-wave instability. Even though the plasma conditions in this setup are slightly different from that of the previous experiment due to a different end plate, the results obtained here show some similarities. The goal here is thus to link the fluctuations inside the main plasma column to those in the SOL as a function of the axial magnetic field. Inside the plasma, we perform a poloidal cut of the light-intensity fluctuations at a radius about 2 cm from the center. For each image, the poloidal wave-number spectrum is determined by Fourier transform of the poloidal cut signal. The average poloidal mode number can thus be assessed as
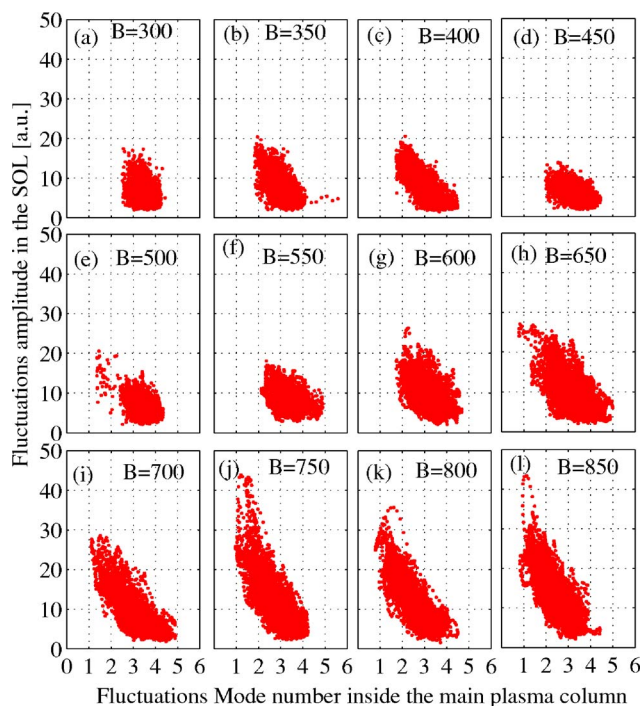
$$m = \frac{a}{\langle k_\theta \rangle} = \frac{a}{\int dk_\theta k_\theta S(k_\theta) / \int dk_\theta S(k_\theta)}$$

and forms the x axis of Fig. 10. The y axis represents the fluctuations at a given point in the SOL at about 6 cm from the center. For low B field, only high mode numbers exist and fluctuations in the SOL are close to the standard deviation. This is indicative of the absence of intermittent bursts that leads to fluctuations several times the standard deviation. As B is increased, two things happen: (i) the onset of low poloidal mode numbers inside the main plasma, and (ii) the onset of large deviations that exceed several times the standard deviation. In other words, and once again, it is shown that there is a correlation between the low poloidal mode number inside the main plasma and the existence of avaloids outside. Moreover, this relationship depends on the magnetic field that leads to the absence of avaloids at low values that are typically below 450 G.

We deduce that the main magnetic field plays a role in generating avaloids by the mean of the $m=1$ poloidal mode number. As B increases, the $m=1$ mode is destabilized, leading to the onset of avaloids.

VII. CONCLUSIONS

We have used fast imaging on the linear plasma CSDX to investigate the spatio-temporal properties and origin of convective events in the SOL of the CSDX linear plasma device. We used several camera views in order to study the

core, the SOL, and the link between the two regions in a rather detailed fashion. The exposure time was set to 1 μs and the time between frames to 10 μs.

Because most of the results obtained in previous publications were made using a Langmuir probe, it was important to show that good agreement exists between time series of the probe and the camera. This was done in two ways. The cross-correlation amplitude between the probe and the camera signals was determined and found to be about 0.5. This amplitude is high considering the differences between the two diagnostic. To understand the reason why the correlation amplitude is still far from 1, we compared the fluctuation statistical properties and found excellent agreement for spatial scales that are greater than 2.5 mm. The small-scale, hence high-frequency, fluctuations are thus not resolved by the camera, mainly due to line integration giving rise to the 0.5 value of the cross-correlation coefficient.

Next, we studied the dynamics inside the main plasma with the focus on properties related to avaloid generation. It was found that different modes exist at different times and the core plasma is in continuous evolution from one mode to another with a transient time about 150 μs. Consequently, the power spectrum does not reflect stationary fluctuations in the sense that its complex form reflects the complexity of the fluctuations occurring all the time, but rather reflects the sum of the individual modes occurring at different times.

Outside the main plasma column, we investigated the properties of avaloids in CSDX. The main finding in this region is the fact that bursts do not detach from the main plasma column. This is a major shift in our understanding of avaloids, as until now it was *imagined* that they have a blobby aspect that is more or less round but most of all that they detach from the main plasma. The link between inside and outside the main plasma column is thus maintained. The lifetime of these intermittent or semiperiodic[8] events depends on the source that is the main plasma not only in the early phase of formation but throughout their existence. The spatio-temporal properties of avaloids were determined statistically and are in good agreement with the Langmuir probes. The only issue is the radial length scale, which is clearly larger than previously estimated because the assumption that it is a blob, or a detached structure with more or less circular cross section, is not valid.

The other main contribution is the understanding of avaloid generation at least in linear devices. In agreement with previous studies made on PISCES, imaging plasma on CSDX has revealed the link between events in the far SOL and an instability at the plasma edge. This was done in different ways. First, we showed that the temporal dependence of the mode numbers and fluctuations in the far SOL are correlated in the sense that high-intensity fluctuations in the SOL are observed when low mode numbers are reported inside the main plasma column. In the second investigation, we used conditional averaging to reveal that it is the $m=1$ poloidal mode number inside the main plasma column that is giving rise to the high-intensity bursts in the far SOL. Finally, we showed that a threshold exists for the onset of the convective structures as the main magnetic field is increased.

VIII. RELATING THE ABOVE RESULTS TO TOROIDAL DEVICES

The question now is how the above results are related to avaloids in tokamaks. First, let us start discussing the dynamics inside the main plasma. The power spectra determined in linear and toroidal devices were always assumed to reflect "stationary" fluctuations. What was shown here is that this assumption is false for CSDX. This assumption has to be rechecked for other linear and toroidal devices. Consequently, it is not excluded that the same thing happens in tokamaks where different high-m poloidal mode numbers may be occurring at different times and the plasma is transiting from one m number to another. This should be the source of future investigations.

Concerning the properties of avaloids in the SOL, it was shown that they do not detach from the main plasma. This can also takes place in tokamaks. The similarity of the autoconditional curves in various tokamaks and in CSDX, fast increase, and a slow decay may reflect this fact. To our knowledge, there is still no clear proof that convective events in the SOL actually detach from tokamak plasmas. This question is very hard to answer using Langmuir probes as they are spatially localized. However, using a battery of 8 $\times$ 8 probes, similar results were obtained by Mistral,[21] where the structures in the SOL remained attached to the main plasma. Imaging may provide the answer. Recently, efforts were dedicated to this issue on Alcator CMOD,[22,23] MAST,[16] and NSTX[24] using high-speed cameras. In all of these images, and because the light intensity naturally decreases around the separatix as neutrals become completely ionized inside the LCFS, it is hard to conclude whether detachment is actually occurring from the main plasma. In other words, it will always look as if the structures are detaching even when they are not. Therefore, this issue should also be a source of future work by investigating regions far from the LCFS where the problem of full ionization and thus the light source is minimized. This is important since if they do not detach, the interaction between the edge and the SOL in tokamaks remains important throughout the avaloids' lifetime. Moreover, and as in CSDX, one can imagine that in tokamaks the ejection of avaloids is related to a particular poloidal mode number that is of course much greater than unity but may be smaller than those associated with drift-wave turbulence.

[1] S. J. Zweben and R. W. Gould, Nucl. Fusion **25**, 171 (1983).
[2] R. Jha, P. K. Kaw, S. K. Mattoo, C. V. S. Rao, Y. C. Saxena, and the ADITYA team, Phys. Rev. Lett. **69**, 1375 (1992).
[3] M. Endler *et al.*, Nucl. Fusion **35**, 1307 (1995).
[4] R. A. Moyer, R. D. Lehmer, T. E. Evans, R. W. Conn, and L. Schmitz, Plasma Phys. Controlled Fusion **38**, 1273 (1996).
[5] B. LaBombard, M. V. Umansky, R. L. Boivin, J. A. Goetz, J. Hughes, B. Lipschutz, D. Mossessian, C. S. Pitcher, and J. L. Terry, Nucl. Fusion **40**, 2041 (2000).

[6] G. Y. Antar, S. I. Krasheninnikov, P. Devynck, R. P. Doerner, E. M. Hollmann, J. A. Boedo, S. C. Luckhardt, and R. W. Conn, Phys. Rev. Lett. **87**, 065001 (2001).

[7] G. Antar, G. Counsell, Y. Yu, B. LaBombard, and P. Devynck, Phys. Plasmas **10**, 419 (2003).

[8] G. Antar, Phys. Plasmas **10**, 3629 (2003).

[9] G. Y. Antar, Phys. Plasmas **13**, 052508 (2006).

[10] G. Antar, P. Devynck, X. Garbet, and S. C. Luckhardt, Phys. Plasmas **8**, 1612 (2001).

[11] S. I. Krasheninnikov, Phys. Lett. A **283**, 368 (2001).

[12] D. L. Rudakov, J. A. Boedo, R. A. Moyer *et al.*, Plasma Phys. Controlled Fusion **44**, 717 (2002).

[13] Y. H. Xu, S. Jachmich, R. R. Weynants, and the TEXTOR team, Plasma Phys. Controlled Fusion **47**, 1841 (2005).

[14] B. P. van Milligen, R. Sanchez, B. A. Carreras, V. E. Lynch, B. LaBombard, M. A. Pedrosa, C. Hidalgo, B. Goncalves, R. Balbin, and W.-A. Team, Phys. Plasmas **12**, 052507 (2005).

[15] T. A. Carter, Phys. Plasmas **13**, 010701 (2006).

[16] G. Y. Antar, G. Counsell, J.-W. Ahn, Y. Yang, M. Price, A. Tabasso, and A. Kirk, Phys. Plasmas **12**, 032506 (2005).

[17] R. Doerner, M. Baldwin, and R. Causey, J. Nucl. Mater. **342**, 63 (2005).

[18] M. J. Burin, G. R. Tynan, G. Y. Antar, N. A. Crocker, and C. Holland, Phys. Plasmas **12**, 052320 (2005).

[19] G. Antar, Phys. Rev. Lett. **91**, 055002 (2003).

[20] G. Y. Antar, G. Counsell, and J.-W. Ahn, Phys. Plasmas **12**, 082503 (2005).

[21] R. Barni, C. Riccardi, T. Pierre, G. Leclert, A. Escarguel, D. Guyomarc'h, and K. Quotb, New J. Phys. **7**, 225 (2005).

[22] S. J. Zweben, D. P. Stotler, J. L. Terry *et al.*, *Proceedings of Invited Papers, 43rd Annual Meeting of the APS Division of Plasma Physics, Long Beach, 2002* (AIP, 2003), Vol. 9, p. 1981.

[23] J. L. Terry, S. J. Zweben, K. Hallatschek *et al.*, Phys. Plasmas **10**, 1739 (2003).

[24] S. J. Zweben, R. J. Maqueda, J. L. Terry *et al.*, Phys. Plasmas **13**, 056114 (2006).